Available online at www.sciencedirect.com

Manufacturing Letters

Manufacturing Letters 00 (2022) 000–000

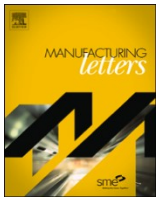

50th SME North American Manufacturing Research Conference (NAMRC 50, 2022)

Investigating Autoregressive and Machine Learning-based Time Series Modeling with Dielectric Spectroscopy for Predicting Quality of Biofabricated Constructs

Shohanuzzaman Shohan[a,b], Mahmud Hasan[a], Binil Starly[a,b,c], Rohan Shirwaiker[a,b,c*]

[a]*Edward P. Fitts Department of Industrial and Systems Engineering, North Carolina State University, Raleigh, NC 27695, United States of America*
[b]*Comparative Medicine Institute, North Carolina State University, Raleigh, NC 27695, United States of America*
[c]*Joint Department of Biomedical Engineering, North Carolina State University and University of North Carolina at Chapel Hill, Raleigh, NC 27695, United States of America*

* Corresponding author. Tel.: +1-919-515-6416; *E-mail address:* rashirwaiker@ncsu.edu

Abstract

Advances in biofabrication processes need to be complemented with appropriate nondestructive quality engineering techniques that can be integrated into scalable engineered tissue manufacturing systems. Previous studies have demonstrated the feasibility of dielectric spectroscopy (DS) as a inline, real time biological quality monitoring alternative. Time series modeling can help improve the efficiency and accuracy of quality prediction by analyzing trends in DS data as the biofabricated constructs mature over time. These models can help forecast potential future deviations in quality attributes and provide opportunities to take preemptive, corrective actions, leading to better yields and higher quality of final products. In this study, we investigated time series modeling of DS data to characterize the effects of two critical biofabrication parameters on constructs of gelatin methacryloyl (GelMA) hydrogel containing human adipose-derived stem cells (hASC) over 11 days of in vitro culture. The performance of standard autoregressive time series models (Exponential Smoothing, ARMA, ARIMA, SARIMA) and conventional sequence-based machine learning (ML) models (SVM, ANN, CNN and LSTM) were analyzed to forecast trends in $\Delta\varepsilon$, a key DS metric that directly correlates to the volume of viable cells in constructs. The ML-based time series models, in general, showed superior performance in predicting future trends in $\Delta\varepsilon$, with LSTM providing the lowest least mean square errors (MSE) in $\Delta\varepsilon$ forecasts. The outcomes of this study highlight the benefits of using DS and time series modeling synergistically for efficient quality monitoring in biofabrication.

Keywords: Time Series Analysis; Machine Learning; Non-destructive Quality Monitoring; Dielectric Spectroscopy; Tissue Engineering

1. Introduction

Recent advances in biofabrication have accelerated the prospect of fabricating patient-specific tissue-engineered medical products (TEMPs) with functional properties similar to natural tissues and organs [1–4]. To enable the scale-up production of TEMPs, scalable non-destructive quality monitoring technologies are essential to track the changes in biological critical quality attributes (CQA) such as cell viability (i.e., proportion of living cells), proliferation (i.e., increase in the number of cells over time), and cell differentiation (i.e., functional or phenotypical changes) in real time. However, majority of the current quality evaluation techniques are predominantly offline and destructive in nature [5]. Other available non-destructive approaches are primarily dependent on analyses of optical images and video feeds [6–8]. These visuals-based approaches can provide information about overall tissue growth but lack the ability to detect changes occurring

inside the constructs over time. Dielectric spectroscopy (DS) is one of the non-image analysis-based altenatives being investigated recently to oversome these limitations.

DS utilizes the dielectric response of living cells to interpret their attributes, as shown in Fig. 1. The phospholipid bilayer cell membrane causes viable cells to polarize in the presence of an alternating electric field, and the intensity of the polarization depends on the frequency. In this phenomenon known as the Maxwell–Wagner effect [9-10], positive and negative charges accumulate at the permeable cell membranes, which results in charge build-up (i.e., permittivity) [11]. Increasing the frequency results in a decrease in the permittivity following a typical trend characterized by three dispersion regions (Fig. 1(b)). For mammalian cells, frequencies between 150-2500 kHz produce the signature β-dispersion trend – steady drop in permittivity with increasing frequency [12-13]. At frequencies below 150 kHz (α-dispersion), a negligible amount of polarization takes place, whereas at frequencies over 2500 kHz (γ-dispersion), the cells do not have sufficient time to polarize. In β-dispersion, the Δε (i.e., the difference between permittivity at the highest and lowest frequencies) is a useful measure of CQA of engineered tissue constructs. From literature, it is known that the Δε is proportional to the volume of viable cells [9-11].

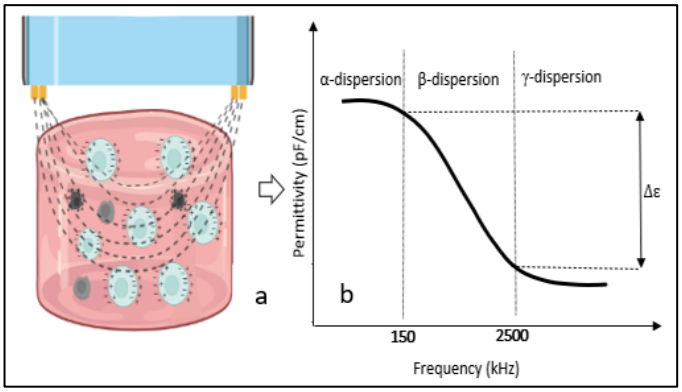

Fig. 1(a). Schematic showing polarization of viable cells encapsulated in engineered tissue induced by DS method (b) Characteristic DS spectrum highlighting the delta permittivity (Δε).

We have recently demonstrated the effectiveness of using Δε in determining overall viability and proliferation of cells in biofabricated constructs [5,14]. Changes in biofabrication parameters and culture conditions can significantly affect the morphological changes and intercellular communication, which also influences the trends in Δε over time [15]. Forecasting of Δε over time as a function of the construct fabrication and culture conditions can enable to preemptively detect potential future deviations in quality and provide an opportunity to take appropriate early corrective actions. From an economics perspective, predicting future Δε could also help save resources by not having to produce irretrievable defective products with imminent fabrication errors.

Traditional forecasting-based time series models have been widely investigated in the literature due to their accuracy in predicting future events. Among these, exponential smoothing [16], autoregressive moving average (ARMA) [17], [18], autoregressive integrated moving average (ARIMA) [19], and seasonal autoregressive integrated moving average (SARIMA) [20], have been typically used for time series data analysis in healthcare and biotechnology industry [21]. The more traditional support vector machine (SVM)-based machine learning (ML) models have also been widely used for time series prediction in biomedical applications [22-23]. More recently, neural networks and deep learning (DL) approaches have been investigated in the biomanufacturing domain. For example, DL models such as artificial neural networks (ANN) and convolutional neural network (CNN) have been utilized for image processing, resolution augmentation, segmentation, and optimization of in situ fabrication parameters in tissue engineering [24-25]. DL-based time series models, including recurrent neural network (RNN) and long short-term memory (LSTM), have also been successfully applied for monitoring of upstream cultivation processes in biopharmaceutical manufacturing [26] and as forecasting and generation tools to aid in therapeutic biologics manufacturing [27].

Process parameters used during biofabrication impact the quality of the engineered tissue constructs. For example, during the biofabrication of constructs using photocrosslinkable hydrogels such as gelatin methacryloyl (GelMA), the duration of exposure to ultraviolet (UV) radiation to achieve photo-crosslinking can significantly impact the mechanical and biological properties of constructs [28-30]. Similarly, culture parameters such as the volume of media during the maturation of constructs [31-32] also affect the viability and proliferation of cells. In this study, we investigated time series modeling with DS to characterize the effect of the two critical biofabrication parameters (UV exposure duration and culture media volume) on the quality of GelMA constructs containing human adipose-derived stem cells (hASC) over 11 days of in vitro culture. The performances of standard autoregressive time series models (exponential smoothing, ARMA, ARIMA and SARIMA) and sequence-based ML models (SVM, ANN, CNN, and LSTM) while forecasting future Δε trends for constructs fabricated under different biofabrication conditions were assessed. To the best of our knowledge, this is the first study focused on DS and time series modeling-driven non-destructive quality forecasting of 3D biofabricated tissue constructs.

2. Methods and materials

2.1. Biofabrication and traditional viability evaluation of GelMA constructs

Human adipose-derived stem cells (hASC) were cultured in 88% v/v MesenPro RS basal media, 10% v/v Mesenpro growth supplement, 1% Glutamax, and 1% antibiotic-antimycotic (Thermo Fisher Scientific, MA) in 175 cm^2 cell culture flasks at 37°C and 5% CO_2. At 80% confluency, cells were passaged until the required cell quantity was achieved. A 5% w/v GelMA solution was prepared by mixing Dulbecco's Phosphate-Buffered Saline (DPBS) (Genesee Scientific, CA) with sterile lyophilized GelMA (60% degree of substitution, MilliporeSigma, MA). Cells ($0.5x10^6$ hASC/ml) were mixed with the GelMA solution to constitute the bioink. Following the experimental design in Table 1, constructs (n = 3/group) were fabricated by photocrosslinking (405 nm UV, 10mW/cm^2) 2 mL bioink/well in untreated 6-well plates (Fig. 2(a)) and then

cultured (37°C, 5% CO_2) over 11 days, with media changes once every 24 hours.

Cell viability was evaluated on day 11 using the standard Live/Dead assay (Thermo Fisher Scientific). Briefly, constructs were washed twice with DPBS and incubated for 45 minutes in 1 ml of DPBS containing 2 µl EthD-I and 0.5 µl calcein AM. Then the solution was aspirated off, and images of the constructs were recorded using an inverted fluorescence microscope (Leica Microsystems, Germany).

Table 1. Experimental design: parametric variations in different construct groups

Group	UV exposure duration (sec)	Media volume (ml)
1	4	2
2	4	4
3	7	2
4	7	4

2.2. DS Assessment

A flush probe (Ø25 mm, Aber Instruments, UK) was used to perform DS on each construct once every 24 hours over 11 days. During each measurement, the probe was introduced into the construct well using a 3D printed custom guide to ensure identical placement of the probe throughout the study, as shown in Figure 2(b). A constant distance of 2 mm was maintained between the top of the GelMA construct and electrodes on the bottom surface of the probe. At each time point (i.e., once every 24 hours over 11 days), one DS measurement was performed. One DS measurement refers to a series of 20 frequency scans (50-20,000 kHz; default frequency range of the equipment). For each group, this resulted in 60 spectral readings (20 frequency scans × 3 constructs/group) per time point. After data collection, permittivity data in the 150-2500 kHz range, which is the relevant β-dispersion for mammalian cell characterization [12,13], was extracted. The Δε of each group at each time point was calculated as the average of the difference between permittivities at 150 and 2500 kHz from the 60 spectral readings. Finally, two-way ANOVA and Tukey's HSD post hoc tests (α = 0.05) were conducted to evaluate the effects of parametric variations and time points on Δε.

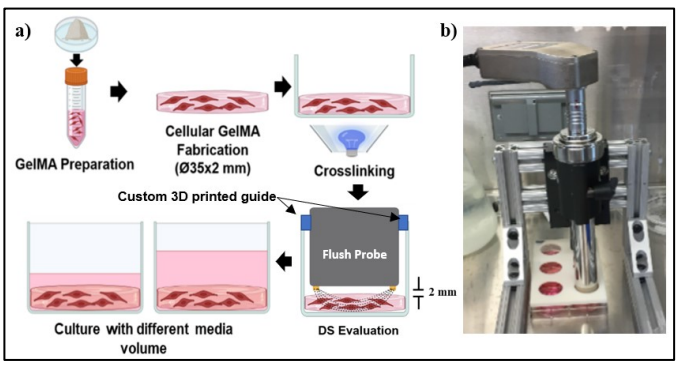

Fig. 2(a). Fabrication, DS evaluation, and culture of hASC cell encapsulated GelMA constructs. (b) Placement of DS probe over samples

2.3. Time Series Modelling

2.3.1. Autoregressive models

To prepare the dataset for subsequent autoregressive time series analysis, the stationarity of the dataset was evaluated using the augmented Dickey-Fuller test. After the data was confirmed as stationary, the dataset was split into train/test, where data collected in the first 9 days (9 days × 60 readings/group × 4 groups = 2160 total readings) were used to train the time series algorithms, and the prediction task was performed for Δε of last 2 days (2 days × 60 predictions/group × 4 groups = 480 total predictions). For exponential smoothing, Holt's Winters Seasonal Exponential Smoothing model was deployed from the python statsmodel library. Dataset was decomposed to check the trend, cycle, seasonality, and noise components. The decomposition results indicated additive seasonality with a sessional period of 60 readings/day/group). For ARMA, ARIMA, and SARIMA analyses, 'pmdarima' python package was utilized to identify the optimal values for trend elements (p, d, q) and seasonal elements (P, D, Q, m = 60), where p, d, and q are the trends in autoregression order, difference order, and moving average order, respectively, and P, D, Q, and m are the seasonal autoregressive order, seasonal difference order, seasonal moving average order, and number of time steps each day, respectively. Finally, the predicted Δε were compared with actual values from the last 2 days for each group using mean square error (MSE).

2.3.2. ML models

Extending the time series analysis of section 2.3.1, the performance of ML-based time series modeling techniques that capture temporal information in sequential Δε data were investigated. The time series Δε trends of the four groups representing the biofabrication parametric variations were subjected to identical data preprocessing techniques before ML models were fit on the data. As an example, Fig. 3 shows the Δε trend of Group 1 (Table 1); the total of 660 data points correspond to 60 readings/time point × 11 time points.

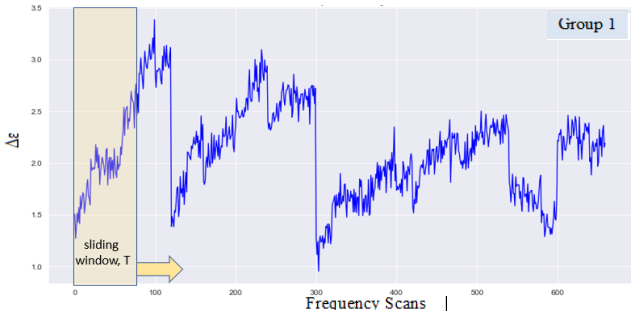

Fig. 3. Δε trend of Group 1

Under the paradigm of supervised ML modeling, the dataset was split into 2 sets – the training set comprising of the first 330 data points of the time series trend and the testing set comprising of the next 330 data points. This splitting approach, despite being in contrast to the one used for the autoregressive models, was adopted to cater to larger training and testing sets usually required for ML models. These two sets were extracted

to train the candidate ML models and to validate their performance on a hold-out test set, respectively. Owing to the time series nature of the data, a randomly split training and testing set extraction was not an option as that would not have retained the temporal characteristics of the data, which is paramount for time series ML models. The splitting of the datasets was done in such a manner that both the training and testing sets had significant trend and seasonality features, the patterns of which could be easily discernible by trained ML models. However, once the training and testing sets were carved out, shuffling was imposed during training to ensure that the ML models were not biased by the sequence of data being fed to them.

To generate the features and targets of the dataset within each subset of data, a sliding window of size T (yellow region in Fig. 3) was scanned across the entire span of the subset. The scan was made at an incremental step size of 1-time unit (i.e., 30 sec) so as to lead to the formation of feature-target pairs wherein each feature is a set of Δε values of size T and the target corresponding to that feature is the next Δε value in the time series trend that will need to be predicted. Quite evidently, this sliding window size of T that dictates the size of the features is a hyperparameter that requires tuning for each dataset. In the case of the Δε data, a size of T = 10 was chosen as a suitable window size that was sufficient to capture correlations between adjacent data points. One conventional ML model (SVM) and three candidate DL models (ANN, CNN, LSTM) were chosen to perform time series prediction on the preprocessed Δε data.

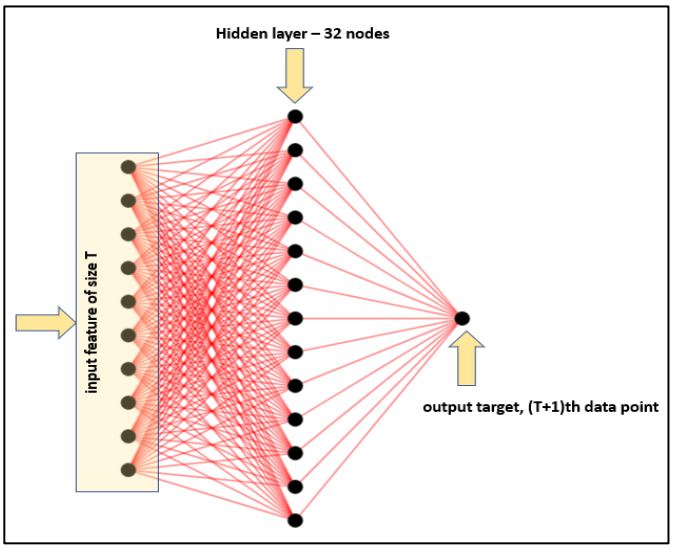

Fig. 4. Fully connected configuration of ANN

Fig. 4. shows a schematic of the fully connected ANN that was trained on the Δε dataset. Features extracted from the sliding window of size T were supplied as inputs from the training set that the ANN trained on. Subsequent values in the time series, i.e., the data with position T+1 in the series, were supplied as the target to be predicted, which explains the uni-nodal output of ANN. As the sliding window continued scanning through the training set from left to right in incremental steps of 1, more sets of training data of size T were generated and subsequently supplied as input data to the ANN.

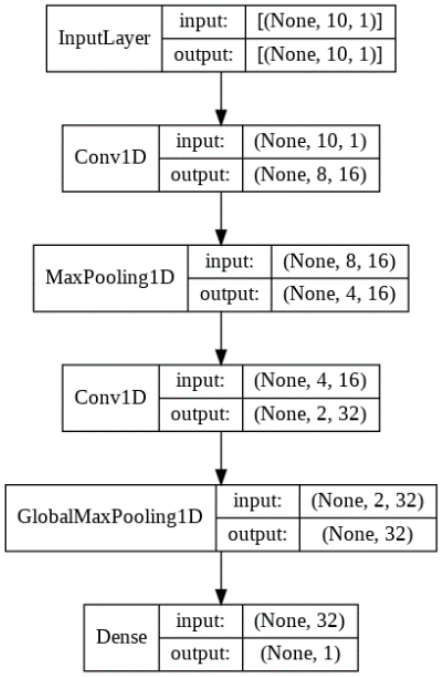

Fig. 5. Network architecture of CNN used in time series modeling

Fig. 5 shows the network configuration of the CNN that was trained on the Δε dataset. It can be observed that the architecture chosen for the CNN comprises of 1-dimensional convolutional layers of varying filter sizes, appropriate for sequence data modeling. The overall architecture comprises of MaxPooling layers sandwiched between the convolutional layers to extract averaged information inherent in the sequence data. Similarly, Fig. 6 shows the architecture for the LSTM model used to train on the Δε data. With reference to Figs. 5 and 6, it can be observed that each layer has an input and output signifying the number of neural network node connections. This is also represented by the accompanied shape tuple in parentheses. The 'None' value in the tuple represents the batch size of data points used during training. The next number in the tuple represents the number of nodes in the layer, and the last number signifies the number of channels of the layer employed to extract information from the data. The 'Dense' layers in both networks represent the output layer responsible for estimating a continuous value.

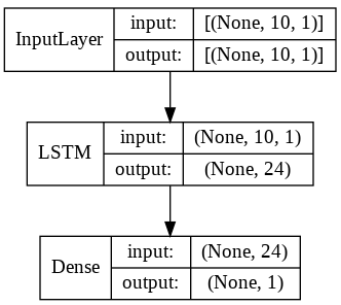

Fig. 6. Network architecture of LSTM used in time series modeling

The LSTM architecture shows a simple single-layer LSTM structure with 24 as its hidden state dimension, which was sufficient to capture temporal information of the time series data. The decision on the number of nodes in the hidden layers

of the ANN, number of filters and maxpooling layers in the CNN architecture, and number of neurons in the hidden state of the LSTM model were all obtained through a series of trial and errors that yielded the best performances across the models. For the LSTM model training, trial ranges of 2-30 and 1-5 were imposed on the number of neurons and number of LSTM layers, respectively. The ranges used were rather conservative owing to the fact that the size of the input dataset was comparatively smaller in contrast to conventional sequence modeling tasks.

For the SVM model, a typical support vector regressor model was used to extract the correlation of the time series trends through an inherent linear autoregressive model. Autoregressive models primarily model the relation of future values to past values in a sequence through linear combinations of the past values. Therefore, a support vector regressor model with a linear kernel exhibiting similar characteristics of target and input variable relationship ought to produce comparable results. This was evident from the kernel that gave the SVM model the best results in terms of lowest MSE. A linear kernel was sufficient to give the best outcomes proving the hypothesis that a linear autoregressive model was apt in modeling the relationship between the data points.

3. Results and discussion

3.1. Δε characteristic of GelMA constructs with different biofabrication parameters

Fig. 7(a) summarizes the trends in Δε for the four construct groups over 11 days. Although the initial cell quantity was identical in all constructs, the Δε magnitude and trends differed over time across groups.

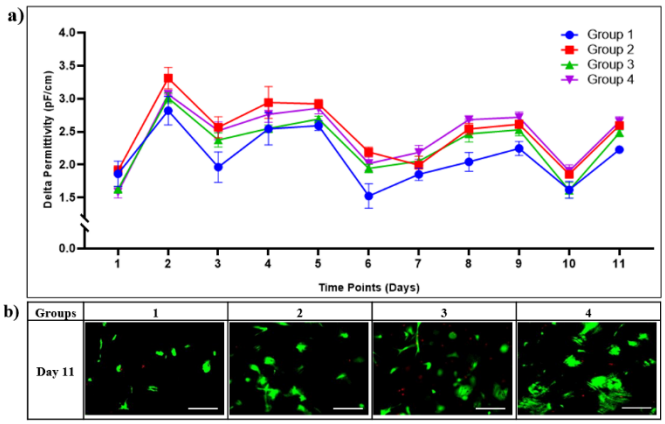

Fig. 7(a). The Δε trends (mean and standard deviation) over 11 days for the four groups. (b) Representative Live/Dead images for each group on day 11 (scale bar 300 μm).

Results of two-way ANOVA showed a significant effect of the parameter combination and time point on Δε ($p < 0.05$). The relatively higher Δε over time for Groups 2 and 4 indicates higher volume of viable cells in those constructs. This conforms to the expectation, given that these constructs received more nutrients due to the higher media volume during culture compared to Groups 1 and 3. A cyclic trend was observed in the Δε magnitudes for all groups, which is also expected from constructs cultured under static, in vitro conditions [33-34]. This trend is reflective of the depletion of nutrients available to cells over time between media changes The Live/Dead images in Fig. 7(b) (green indicating live cells, red indicating dead cells) at Day 11 aligns with the trends noted in Δε. The lowest intercellular communication was observed in Group 1, which also aligns with the lowest Δε magnitude observed for Group 1 over time.

3.2. Time series prediction performance of models

Performance (MSE) of different autoregressive time series models in predicting Δε for each of the four groups is summarized in Table 2. It was observed that by introducing seasonality (SARIMA), the prediction performance of the time series models improved significantly for all groups. However, despite the improvement in model performance due to the introduction of seasonality, the prediction accuracy was multiple folds higher for the ML-based time series models, which is evident from the MSE values in Table 3.

Table 2. Prediction performance (MSE) of autoregressive time series models

Group	Exponential Smoothing	ARMA	ARIMA	SARIMA
1	0.2381	0.1703	0.2875	0.1976
2	0.3345	0.3894	0.3789	0.3072
3	0.7561	0.4181	0.4181	0.4145
4	0.1446	0.1926	0.1926	0.1445

Table 3. Prediction performance (MSE) of ML-based time series models

Group	SVM	ANN	CNN	LSTM
1	0.0297	0.02418	0.02942	0.02240
2	0.0347	0.03343	0.04287	0.03203
3	0.0401	0.03019	0.03566	0.02956
4	0.0343	0.02451	0.03031	0.02475

Since the autoregressive and ML models were all employed to predict continuous Δε values of the future, this was quite evidently a regression task, and hence the MSE score was an appropriate evaluation metric for the models. While all the ML models were comparable in their performances in forecasting Δε trends in the testing set, LSTM had the lowest mean MSE value across all groups (Table 3). This is also evident in Fig. 8 that shows the Δε trends of the testing set overlaid on the trends predicted by the three DL models for Group 1. These graphs show that, for the most part, the trends predicted by ANN overshoot while the CNN predictions undershoot and lag the actual Δε trend of the testing set. In comparsion, the LSTM-predicted trends align well with the actual data. This can be attributed to the ability of the LSTM to capture long term dependencies in temporal data through memory cells, which allows the models to capture any long term autoregressive relationship in the Δε data. The superior performance of the ML/DL models for this prediction aligns with similar investigations in previous literature [35]. The comparatively poorer performance of the autoregressive models in predicting the time series Δε data can be attributed to the absence of strong

seasonality patterns in the data to which such parametric methods are typically more responsive. Consequently, ML models which do not rely on such assumptions perform better in extracting the regression relationship. It is to be noted that, the ML models perform a one step ahead prediction on the test data, and hence do not recursively use the predicted results from a previous iteration as new input for the model to do prediction on the step ahead. This allows for prediction errors to not build up and deviate future predicted values by large amounts. While a recursive input of previously predicted values would have been more appropriate for a multi-step forecast, for the use case in this study, a one step ahead prediction is commensurate to the frequency at which data is collected.

4. Conclusion

In this study, we invaestigated the application of time series modeling for assessing the effects of two biofabrication parameters (UV exposure duration and media volume) on the key DS metric of Δε, which is correlated to the viability and proliferation of cells in engineered tissue constructs. The results showed that there was a significant variation in the trends in Δε of the four groups of constructs fabricated using different process parameter combinations, which was in agreement with results of a traditional biochemical assessment assay. The results of time series analyses using standard autoregressive and ML-based models to forecast Δε showed that ML models showed consistently better prediction performance than autoregressive models. The LSTM model outperformed (lowest MSE) all other models tested. The approach and outcomes of this study demonstrate the capability of DS and time series modeling for efficient predictive quality monitoring of engineered tissues.

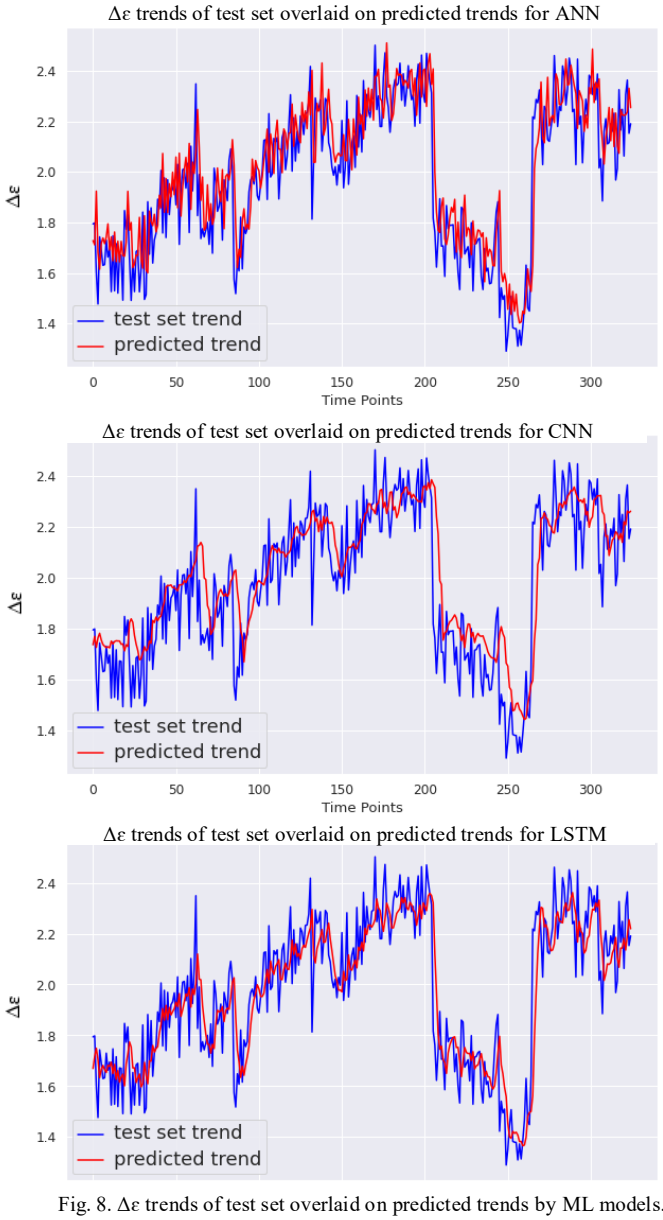

Fig. 8. Δε trends of test set overlaid on predicted trends by ML models.

Acknowledgments

This research was supported by grants from the Advanced Regenerative Manufacturing Institute (ARMI) BioFabUSA and NSF (CBET-1703466).

References

[1] C. R. Lynch, P. P. D. Kondiah, and Y. E. Choonara, "Advanced strategies for tissue engineering in regenerative medicine: A biofabrication and biopolymer perspective," Molecules, vol. 26, no. 9, p. 2518, May 2021.
[2] P. Chansoria, K. Schuchard, and R. A. Shirwaiker, "Process hybridization schemes for multiscale engineered tissue biofabrication," Wiley Interdiscip. Rev. Nanomedicine Nanobiotechnology, vol. 13, no. 2, p. e1673, Mar. 2021.
[3] L. Moroni et al., "Biofabrication: A Guide to Technology and Terminology.," Trends Biotechnol., vol. 36, no. 4, pp. 384–402, Apr. 2018.
[4] K. Nakayama, "In Vitro Biofabrication of Tissues and Organs," in Biofabrication: Micro- and Nano-fabrication, Printing, Patterning and Assemblies, Elsevier Inc., 2013, pp. 1–21.
[5] L. K. Narayanan, T. L. Thompson, A. Bhat, B. Starly, and R. A. Shirwaiker, "Investigating Dielectric Impedance Spectroscopy As a Non-Destructive Quality Assessment Tool for 3D Cellular Constructs," 2017.
[6] A. A. Appel, M. A. Anastasio, J. C. Larson, and E. M. Brey, "Imaging challenges in biomaterials and tissue engineering," Biomaterials, vol. 34, no. 28. Elsevier, pp. 6615–6630, 01-Sep-2013.
[7] S. B. Kim et al., "A mini-microscope for in situ monitoring of cells.," Lab Chip, vol. 12, no. 20, pp. 3976–3982, 2012.
[8] Z. Wang et al., "A High-Resolution Minimicroscope System for Wireless Real-Time Monitoring," IEEE Trans. Biomed. Eng., vol. 65, no. 7, pp. 1524–1531, Jul. 2018.
[9] D. A. McRae and M. A. Esrick, "Deconvolved electrical impedance spectra track distinct cell morphology changes," IEEE Trans. Biomed. Eng., vol. 43, no. 6, pp. 607–618, Jun. 1996.
[10] A. Angersbach, V. Heinz, and D. Knorr, "Electrophysiological model of intact and processed plant tissues: Cell disintegration criteria," Biotechnol. Prog., vol. 15, no. 4, pp. 753–762, Jul. 1999.
[11] G. G. Matthews, "Electrical Properties of Cells," in Cellular Physiology of Nerve and Muscle, Malden, MA USA: Blackwell Publishing Ltd., 2013, pp. 216–224.
[12] S. Ansorge, G. Esteban, and G. Schmid, "On-line monitoring of infected Sf-9 insect cell cultures by scanning permittivity measurements and comparison with off-line biovolume measurements," Cytotechnology, vol. 55, no. 2–3, pp. 115–124, Dec. 2007.
[13] C. Cannizzaro, R. Gügerli, I. Marison, and U. von Stockar, "On-line biomass monitoring of CHO perfusion culture with scanning dielectric spectroscopy," Biotechnol. Bioeng., vol. 84, no. 5, pp. 597–610, Dec. 2003.
[14] S. Shohan, J. Harm, M. Hasan, B. Starly, and R. Shirwaiker, "Non-destructive quality monitoring of 3D printed tissue scaffolds via dielectric impedance spectroscopy and supervised machine learning," Procedia Manuf., vol. 53, pp. 636–643, Jan. 2021.
[15] L. K. Narayanan, T. L. Thompson, R. A. Shirwaiker, and B. Starly, "Label free process monitoring of 3D bioprinted engineered constructs via

dielectric impedance spectroscopy," Biofabrication, vol. 10, no. 3, p. 035012, Jun. 2018.

[16] C. Yu et al., "Time Series Analysis and Forecasting of the Hand-Foot-Mouth Disease Morbidity in China Using An Advanced Exponential Smoothing State Space TBATS Model," Infect. Drug Resist., vol. 14, p. 2809, 2021.

[17] M. Shardell, A. D. Harris, S. S. El-Kamary, J. P. Furuno, R. R. Miller, and E. N. Perencevich, "Statistical analysis and application of quasi experiments to antimicrobial resistance intervention studies," Clin. Infect. Dis., vol. 45, no. 7, pp. 901–907, 2007.

[18] E. Kontopantelis, T. Doran, D. A. Springate, I. Buchan, and D. Reeves, "Regression based quasi-experimental approach when randomisation is not an option: Interrupted time series analysis," BMJ, vol. 350, Jun. 2015.

[19] M. A. Hagiwara, B. A. Gare, and M. Elg, "Interrupted time series versus statistical process control in quality improvement projects," J. Nurs. Care Qual., vol. 31, no. 1, pp. E1–E8, 2016.

[20] B. Nunes, I. Natário, and M. L. Carvalho, "Time series methods for obtaining excess mortality attributable to influenza epidemics," Stat. Methods Med. Res., vol. 20, no. 4, pp. 331–345, Aug. 2011.

[21] J. E. Ewusie et al., "Methods, applications, interpretations and challenges of interrupted time series (ITS) data: Protocol for a scoping review," BMJ Open, vol. 7, no. 6, Jun. 2017.

[22] W. A. Chaovalitwongse and P. M. Pardalos, "On the time series support vector machine using dynamic time warping kernel for brain activity classification," Cybern. Syst. Anal. 2008 441, vol. 44, no. 1, pp. 125–138, Jan. 2008.

[23] S. Mukherjee, E. Osuna, and F. Girosi, "Nonlinear prediction of chaotic time series using support vector machines," Neural Networks Signal Process. - Proc. IEEE Work., pp. 511–520, 1997.

[24] W. L. Ng, A. Chan, Y. S. Ong, and C. K. Chua, "Deep learning for fabrication and maturation of 3D bioprinted tissues and organs," Virtual and Physical Prototyping, vol. 15, no. 3, pp. 340–358, 2020.

[25] R. Sood, B. Topiwala, K. Choutagunta, R. Sood, and M. Rusu, "An application of generative adversarial networks for Super Resolution Medical Imaging," 2018 17th IEEE International Conference on Machine Learning and Applications (ICMLA), 2018.

[26] J. Smiatek, C. Clemens, L. M. Herrera, S. Arnold, B. Knapp, B. Presser, A. Jung, T. Wucherpfennig, and E. Bluhmki, "Generic and specific recurrent neural network models: Applications for large and small scale biopharmaceutical upstream processes," Biotechnology Reports, vol. 31, 2021.

[27] H. Narayanan, F. Dingfelder, A. Butté, N. Lorenzen, M. Sokolov, and P. Arosio, "Machine Learning for Biologics: Opportunities for protein engineering, developability, and formulation," Trends in Pharmacological Sciences, vol. 42, no. 3, pp. 151–165, 2021.

[28] C. Kim et al., "Stem Cell Mechanosensation on Gelatin Methacryloyl (GelMA) Stiffness Gradient Hydrogels," Ann. Biomed. Eng. 2019 482, vol. 48, no. 2, pp. 893–902, Dec. 2019.

[29] P. Chansoria, S. Asif, N. Gupta, J. Piedrahita, and R. A. Shirwaiker, "Multiscale Anisotropic Tissue Biofabrication via Bulk Acoustic Patterning of Cells and Functional Additives in Hybrid Bioinks," Adv. Healthc. Mater., p. 2102351, 2022.

[30] P. Chansoria, S. Asif, K. Polkoff, J. Chung, J. A. Piedrahita, and R. A. Shirwaiker, "Characterizing the Effects of Synergistic Thermal and Photo-Cross-Linking during Biofabrication on the Structural and Functional Properties of Gelatin Methacryloyl (GelMA) Hydrogels," ACS Biomaterials Science and Engineering, vol. 7, no. 11, pp. 5175–5188, Nov. 2021.

[31] G. Maiorano et al., "Effects of Cell Culture Media on the Dynamic Formation of Protein−Nanoparticle Complexes and Influence on the Cellular Response," ACS Nano, vol. 4, no. 12, pp. 7481–7491, Dec. 2010.

[32] B. Frahm et al., "Determination of dissolved CO2 concentration and CO2 production rate of mammalian cell suspension culture based on off-gas measurement," Journal of Biotechnology, vol. 99, no. 2, pp. 133–148, Oct. 2002.

[33] A. T. Miccheli et al., "NMR-based metabolic profiling of human hepatoma cells in relation to cell growth by culture media analysis," Biochim. Biophys. Acta - Gen. Subj., vol. 1760, no. 11, pp. 1723–1731, Nov. 2006.

[34] G. Gstraunthaler, S. T, and P. W, "Impact of culture conditions, culture media volumes, and glucose content on metabolic properties of renal epithelial cell cultures. Are renal cells in tissue culture hypoxic?," Cell. Physiol. Biochem., vol. 9, no. 3, pp. 150–172, 1999.

[35] S. Kaushik, A. Choudhury, P. K. Sheron, N. Dasgupta, S. Natarajan, L. A. Pickett, and V. Dutt, "Ai in healthcare: Time-series forecasting using statistical, Neural, and Ensemble Architectures," Frontiers in Big Data, vol. 3, 2020.